

# A numerical simulation of a “Super-Earth” core delivery from $\sim 100$ AU to $\sim 8$ AU.

Seung-Hoon Cha and Sergei Nayakshin

*Department of Physics & Astronomy, University of Leicester, Leicester, LE1 7RH, UK*  
*E-mail: seunghoon.cha@astro.le.ac.uk*

Received

## ABSTRACT

We use SPH simulations with an approximate radiative cooling prescription to model evolution of a massive and large ( $\sim 100$  AU) very young protoplanetary disc. We also model dust growth and gas-grain dynamics with a second fluid approach. It is found that the disc fragments onto a large number of  $\sim 10$  Jupiter mass clumps that cool and contract slowly. Some of the clumps evolve onto eccentric orbits delivering them into the inner tens of AU, where they are disrupted by tidal forces from the star. Dust grows and sediments inside the clumps, displaying a very strong segregation, with the largest particles forming dense cores in the centres. The density of the dust cores in some cases exceeds that of the gas and is limited only by the numerical constraints, indicating that these cores should collapse into rocky planetary cores. One particular giant planet embryo migrates inward close enough to be disrupted at about 10 AU, leaving a self-bound solid core of about  $7.5 M_{\oplus}$  mass on a low eccentricity orbit at a radius of  $\sim 8$  AU. These simulations support the recent suggestions that terrestrial and giant planets may be the remnants of tidally disrupted giant planet embryos.

## 1 INTRODUCTION

### 1.1 Two competing theories for planet formation

The currently favored “Core Accretion” paradigm for planet formation (Safronov 1969; Wetherill 1990; Pollack et al. 1996) stipulates that planets grow in a  $R \lesssim 10$  AU scale disc by accumulation of solids into grains and then into km-sized bodies called planetesimals which then collide and merge into ever larger rocky objects. There is a well known difficulty with the paradigm, e.g., the planetesimal assembly step (e.g., Wetherill 1990). Due to gas-grains friction forces, grains are found to migrate radially inwards with velocities strongly dependent on the grain size (Weidenschilling 1977). Small (mm-sized or less) grains are “glued” to the gas and hence co-rotate with it; larger bodies (e.g., km-sized rocks) barely notice drag forces from the gas and thus orbit the star at the local Keplerian speed, which is slightly higher than the gas orbital velocity. The objects in the middle, e.g., about a meter in size, move with respect to gas at velocities approaching a few tens of  $\text{m s}^{-1}$ . Such objects should migrate inward rapidly and be lost to the star. Going from cm-sizes to km sizes is also complicated by the fact that the collisions of  $\sim$  m-sized boulders occur at velocities higher than a few  $\text{m s}^{-1}$ . Experiments show that fragmentation of solids, rather than their growth, is the most likely outcome for such high-speed collisions (Blum & Wurm 2008). Alternatively, gravitational instability of a dense dust layer within a gas-dust disc could form km-sized bodies directly (Safronov 1969; Goldreich & Ward 1973), but turbulence and instabilities are believed to prevent grains from sedi-

menting to the midplane of the disc (Weidenschilling 1980). More recent work suggests that solids may be concentrated into larger structures by instabilities and turbulence in the disc (e.g., Youdin & Goodman 2005; Johansen et al. 2007; Cuzzi et al. 2008), allowing them to rapidly grow to km-sized bodies.

Until very recently, the only serious alternative<sup>1</sup> to the core accretion scenario was the disc gravitational instability (GI) model (Kuiper 1951; Cameron 1978) for giant planet formation, most convincingly formulated, based on hydrodynamical simulations, by Boss (1997). In this model the giant planets form as self-gravitating condensations in a massive protoplanetary disc. Boss (1998) further argued that dust grains inside the young giant planet precursors, which we shall term the giant (planet) embryo, may sediment to the centre and form moderate mass solid cores, as observed. Boss et al. (2002), in addition pointed out that giant planet embryos may lose their gas-rich envelopes by photoevaporation from nearby OB stars.

However, the difficulties of this scenario, initially applied to the Solar System giants, were pointed out by a number of authors. Cassen et al. (1981) argued that the gaseous disc must be unrealistically heavy, e.g., up to  $1 M_{\odot}$ , to collapse gravitationally. Cameron et al. (1982) showed that the thermal bath of the Solar radiation at the location of Jupiter is intensive enough to result in evaporation

<sup>1</sup> One of us was recently made aware of much earlier work on the subject (starting from McCrea 1960), which is discussed more fully below.

and a complete dispersal of a young 1 Jovian (Jupiter) mass self-gravitating gas cloud. Wetherill (1990) stressed the fact that giant planets in the Solar System are significantly more metal rich than the Sun, which could not be the case, in his view, if planets formed from a disc with same metallicity as the star. This constraint is avoided, however, if planets are allowed to lose volatile elements preferentially, as in the model of Boss et al. (2002). But perhaps the strongest objection from the Solar System is that the GI theory does not have an answer to forming terrestrial planets, and hence one must appeal to the core accretion model for these.

In addition, improved theoretical understanding of disc fragmentation and hydrodynamical simulations (Gammie 2001; Rafikov 2005; Rice et al. 2005) showed that protoplanetary discs cannot fragment on clumps on scales less than  $\lesssim 50\text{--}100$  AU from the star. As there is a large number of giant planets observed at AU and even sub-AU distances from their parent stars (e.g., Baraffe et al. 2010), these would seem to rule out the GI formation path. Furthermore, Helled & Schubert (2008) and Helled et al. (2008) found that dust sedimentation in giant embryos is suppressed by vigorous convective motions and the embryos soon become too hot for dust grains to survive. Therefore, the model of Boss (1997, 1998) did not seem to find support from detailed independent simulations.

Therefore the core accretion scenario is by far the most widely accepted model for planet formation at the moment, although the existence of exosolar giant planets at  $R \sim 100$  AU most likely implies that these formed in situ, and hence the GI model cannot be completely excluded (Boley 2009).

## 1.2 The tidal downsizing model

Theoretical work on planet migration (e.g., Goldreich & Tremaine 1980; Tanaka et al. 2002; Bate et al. 2003) and observations of “hot jupiters” too close to the star where they could not have possibly formed (Lin et al. 1996) puts a serious dent in the critiques of the GI model detailed above, and allows for a wholly new look at the planet formation process: if we know that planets can and must, in the case of hot jupiters, migrate in their discs, could all the planets not be born at  $R \gtrsim 50\text{--}100$  AU and then migrate inwards to their observed positions?

Motivated by this, a modified scheme for planet formation has been recently proposed by Boley et al. (2010) and Nayakshin (2010a). In particular, it is suggested that youngest proto-planetary discs are very massive (comparable in mass to their parent star, see Machida et al. 2010; Stamatellos & Whitworth 2008) and extended due to a large angular momentum reservoir of typical molecular clouds (e.g., Goodman et al. 1993). Such discs fragment onto gas clumps with mass of a few to a few tens of  $M_J$  at large distances from the parent star ( $\sim 100$  AU). It is then proposed that the clumps, also referred to as giant planet embryos, migrate inward on time scales of a few thousand years to ten times that. This migration may be related to the “burst mode accretion” discussed by Vorobyov & Basu (2005, 2006, 2010).

In a constant clump (giant planet embryo) mass model, Nayakshin (2010c) have shown that dust is very likely to grow and sediment to the centre of the clump (as earlier suggested by Boss 1998). The vigorous convection that resisted dust sedimentation in Helled & Schubert (2008); Helled et al.

(2008) does not occur in these models exactly because the embryos start from afar. At distances of  $\sim 100$  AU they are initially fluffy and cool, contracting slowly due to radiative cooling. Nayakshin (2010b) continued the calculation into the phase when a massive solid core forms in the centre and found that energetic feedback from growing core onto the surrounding gas may significantly impede further growth of the core.

The final step in this “tidal downsizing” hypothesis is the disruption of the gaseous envelope by tidal or irradiative mass loss when the planet is within a few AU from the star (Nayakshin 2010a). If all the gas envelope is removed then the remnant is a rocky planet; if a part of the massive gas envelope remains then the outcome is a giant planet (see also Boss et al. 2002).

It is interesting to note that except for migration of the embryos, the important parts of the tidal downsizing hypothesis were discussed by a number of authors as early as 50 years ago (!). For example, McCrea (1960) argued that planet formation begins inside “flocules”, and McCrea & Williams (1965) and Williams & Crampin (1971) then have shown that grains could have grown inside and sedimented to the centre, whereas the outer envelope of volatile elements could have been removed by tidal forces of the Sun. However, Donnison & Williams (1975) realised that the tidal dispersal process is extremely rapid, e.g., dynamical, at the present locations of the terrestrial planets, whereas grain sedimentation requires at least  $10^3$  years. Therefore Donnison & Williams (1975) concluded that “terrestrial protoplanets envisaged in this theory are unstable and cannot have existed”. The tidal downsizing hypothesis is thus late by about 30 years, given that planet migration was “invented” by Goldreich & Tremaine (1980).

Neither Boley et al, who simulated numerically gas-only discs, nor Nayakshin, who concentrated on isolated embryos, have actually demonstrated that the hypothesis works in a realistic gas-dust simulation of the process. Our goal here is to carry out a two-fluid hydrodynamical simulation of a massive proto-planetary disc to test whether massive embryos do form with appropriate conditions for dust sedimentation, whether they indeed migrate inward and survive long enough to make it into the inner non-self-gravitating disc. We performed a dozen of such simulations varying the radiative cooling prescription (see below) and initial conditions, indeed finding clump creation and inward migration to be common place processes.

While a full study of the parameter space of the simulations remain to be performed, here we report one particular simulation that, in our view, provides a proof of the concept for the tidal downsizing hypothesis. In this simulation the inward migrating embryo is dense enough to be disrupted only at around 10 AU (and not earlier) and to deposit a  $\sim 7.5 M_{\oplus}$  solid core into a low eccentricity orbit at about 8 AU.

## 2 THE NUMERICAL METHOD

We employ the three-dimensional smoothed particle hydrodynamics (SPH)/N-body code GADGET-3, an updated version of the code presented in Springel (2005). We use adaptive SPH smoothing lengths. The dust component is

modelled by a two-fluid approach somewhat similar to our radiation-transfer scheme reported in Nayakshin et al. (2009), although the scheme is much simpler in the present case.

## 2.1 Dust particles implementation

The dust particles in our approach are collisionless particles that experience two forces, one is the gravity due to the gas, the star and themselves, and the other is the aerodynamic drag force between the dust and the gas particles. The standard GADGET-3, machinery is used to calculate the gravitational acceleration,  $\mathbf{a}_{grav}$ , for all the particles.

To calculate the gas density at the location of the dust particle, we use the standard SPH approach, first finding the distance  $h_d$  such that the sphere of radius  $h_d$ , centered on the dust particle position,  $\mathbf{r}_d$ , contains  $N_{ngb} = 40$  neighbours. The distance  $h_d$  is the “smoothing length” at  $\mathbf{r}_d$ . The gas density,  $\rho_g$ , is then calculated by

$$\rho_g = \sum_j m_j W(|\mathbf{r}_j - \mathbf{r}_d|, h_d) = \sum_j \rho_j, \quad (1)$$

where the summation goes over all the SPH neighbours of the dust particles so defined,  $m_j$  and  $\mathbf{r}_j$  are the mass and the position of particle  $j$ , respectively, and  $W$  is the SPH smoothing kernel (Springel 2005). The quantity  $\rho_j$  is the contribution of the  $j^{th}$  gas neighbour to the gas density around the dust particle, which we shall need below.

Other gas dynamical or thermodynamical properties at the dust particle position are calculated in a very similar way. For example, the gas velocity is given as

$$\mathbf{v}_g = \rho_g^{-1} \sum_j \mathbf{v}_j m_j W(|\mathbf{r}_j - \mathbf{r}_d|, h_d). \quad (2)$$

Eqs. (7-9) of Weidenschilling (1977) are used to calculate the aerodynamic drag force ( $\equiv F_d$ ) on the dust particle. We then also define the dust particle “stopping time”,  $t_s$  due to the drag forces as

$$t_s = \frac{m_d |\mathbf{v}_d - \mathbf{v}_g|}{|F_d|}, \quad (3)$$

(Eq. 10 of Weidenschilling 1977). Having calculated the stopping time, we update the dust particle velocity in an implicit scheme, according to

$$\mathbf{v}_d^{\text{new}} = \left[ \frac{\mathbf{v}_d}{\Delta t_d} + \frac{\mathbf{v}_g}{t_s} + \mathbf{a}_{grav} \right] \left( \frac{1}{\Delta t_d} + \frac{1}{t_s} \right)^{-1}, \quad (4)$$

where  $\Delta t_d$  is the block-sized (in powers of 2) time step for the dust particle. The time step is determined with the usual accuracy criteria for gravity integration (Springel 2005), and also by the condition that the dust particles do not “skip” interactions with the SPH particles (Nayakshin et al. 2009). Note that this scheme recovers the well known results for short dust particle stopping time: if  $t_s \ll \Delta t_d$ ,  $\mathbf{v}_d^{\text{new}} \rightarrow \mathbf{v}_g + \mathbf{a}_{grav} t_s$ .

In order to conserve the momentum in the gas-dust interactions, the momentum loss of a dust particle due to the aerodynamic force,  $\Delta \mathbf{P}_d$ , is passed back to the respective gas particle neighbours with the negative sign. This involves “spreading” of  $-\Delta \mathbf{P}_d$  over all of the neighbours of the dust particle. Following the method of Nayakshin et al. (2009),

this spreading is done proportional to the respective contribution of the particle  $j$  to the gas density,  $\rho_j$ , at the location of the dust particle. The SPH particle  $j$  is then due to receive the momentum “kick”,  $\Delta \mathbf{P}_{d,j}$  given by

$$\Delta \mathbf{P}_{d,j} = -\frac{\rho_j}{\rho_g} \Delta \mathbf{P}_d, \quad (5)$$

where  $\rho_g$  is given by Eq. (1). For each SPH particle, all the interactions with its dust neighbours are counted, defining in this way the total change in momentum due to the dust-gas interactions,  $\Delta \mathbf{P}_j$ . Note that the SPH particle will in general have its own time step  $\Delta t_j$ . Therefore,  $\Delta \mathbf{P}_j$  quantity is additive and is updated also during the time that the SPH particle itself is “inactive” (its time step  $\Delta t_j > \Delta t_d$  of a dust neighbour). For added accuracy, the momentum kick is not passed to the SPH particle directly, but instead is used to define the acceleration acting on the gas particle due to gas-dust drag force,  $\mathbf{a}_j = \Delta \mathbf{P}_j / \Delta t_j$ . This also means that the gas-drag acceleration is used as an additional time-stepping criterium for the SPH particles, ensuring accurate time integration when the gas-drag forces are large.

We emphasize that this scheme is an almost exact copy of the (Nayakshin et al. 2009) approach, who ran a number of simulations designed to test the accuracy of the momentum transfer to the gas.

## 2.2 Dust grain growth

We also implement a simple hit-and-stick dust growth model in the code. Physically, dust particles of different sizes sediment to the centres of the gas clumps or to the disc midplane at different velocities, with larger particles settling faster (e.g., Boss 1998; Dullemond & Dominik 2005). Larger grains thus sweep smaller ones, which then stick to the larger ones. As pointed out by Dullemond & Dominik (2005), if such a simple logic were correct then one would expect that protoplanetary discs would only contain cm-sized particles after just a short time. Instead, small dust particles are clearly observed in the protoplanetary discs, requiring both grain growth and fragmentation.

Such a detailed grain growth model is well beyond the scope of what we can realistically do in this paper. On a numerical level, that would require tracking the smallest microscopic dust particles, and then allowing them to accrete onto the large ones. This would necessitate introduction of dust “sink particles”, and also an uncomfortably large number of “small” dust particles. One would also have to introduce, likely arbitrary, prescriptions for dust fragmentation.

Therefore, we simply assume that, while we explicitly follow the population of larger dust grains, there is always an associated population of microscopically small grains as well. The density of those is taken to be roughly same as that of the large grains in the same location. Following Nayakshin (2010c), dust grains grow at the rate given by

$$\frac{da}{dt} = \left\langle \frac{\rho_d}{4\rho_a} (\Delta v + v_{br}) \right\rangle \left( \frac{v_{\text{max}}}{v_{\text{max}} + \Delta v} \right)^2, \quad (6)$$

where  $a$  is grain size,  $\rho_a = 2 \text{ g cm}^{-3}$  is the material density of grains,  $\rho_d$  is the density of dust around the grains,  $\Delta v$  is the absolute magnitude of the gas-dust velocity difference,  $\Delta v = |\mathbf{v}_d - \mathbf{v}_g|$ ,  $v_{br} = 10 \text{ cm s}^{-1}$  is the Brownian velocity of microscopic grains (cf. Dullemond & Dominik 2005), and

$v_{\max} = 3 \text{ m s}^{-1}$  is the critical velocity above which colliding grains are assumed not to stick (Blum & Wurm 2008). The local dust density,  $\rho_d$ , is calculated in the same way as the gas density around the dust particle location (Eq. 1), but only dust particles are considered as a neighbour.

### 2.3 Gravitational collapse of dust particle condensations

Due to grain sedimentation into the centres of the clumps, the grain population there can become self-gravitating (Boss 1998; Boley et al. 2010; Nayakshin 2010c,b). If point-mass gravity law is used to treat their interactions then such compact grain distributions may collapse to a point. This numerical problem (arising because of the final and fixed mass of the N-body – dust particles) is solved by the introduction of the minimum softening length for the dust particles, as is traditional in most N-body codes (Springel 2005). For the runs presented in this paper we use the minimum gravitational softening parameter of  $h_{\min} = 0.05 \text{ AU}$ .

In contrast, we do not introduce any softening for the dust-gas aerodynamic drag forces. Therefore, we *under estimate* the physical tendency of the self-gravitating grain condensations to gravitational collapse. This means that our results concerning the formation of bound grain condensations are conservative; a better numerical treatment should lead to even tighter bound solid cores.

The gravitational force from the star is also softened on the same 0.05 AU scale. However, as we use a sink particle boundary condition for the star of 1 AU, the gravitational softening of the stellar gravitational force is never important in practice (close particles are accreted, i.e., added to the star, before the softening becomes significant). This also implies that the tidal field of the star is not softened in practice. Hence, just as the argument above, if a self-gravitating dusty core (a collection of a large number of gravitationally self-bound dust particles) survives near the star for a long time despite the tidal forces, we can be confident that this result will stand even at smaller values of  $h_{\min}$ .

### 2.4 Radiative cooling prescription

The radiative cooling scheme we employ follows simple physical considerations. As is very well known from simulations of collapsing molecular clouds (Larson 1969; Masunaga & Inutsuka 2000), low density gas cools rapidly and therefore it is essentially isothermal, with temperature fixed by an external heating rate. The highest density material, on the other hand, is expected to be found inside the giant planet embryos that are optically thick. For definitiveness, we use the Nayakshin (2010c) model for embryos with opacity law  $\kappa = \kappa_0(T/T_0)$ . It turns out that for such an opacity law the cooling time is a few hundred years for plausible opacity values and then increases as the embryo contracts (cf. sections 3.1 and 3.3 in Nayakshin 2010c). Therefore our approximate energy balance equation reads

$$\frac{\partial u}{\partial t} = Q^+ - \frac{u - u_{\text{amb}}}{t_{\text{cool}}(\rho)}, \quad (7)$$

where  $\rho$  is the gas density,  $u$  is the gas internal energy per unit gram,  $Q^+$  includes all the usual hydrodynamical heating terms (compressional heating and artificial viscosity

heating for convergent flows),  $u_{\text{amb}}$  is the ‘‘ambient’’ value for gas in thermal equilibrium with external heating (corresponding to molecular gas held at 10 K for these simulations), and  $t_{\text{cool}}$  is the density dependent cooling time:

$$t_{\text{cool}}(\rho) = t_0 \left( 1 + \frac{\rho}{\rho_{\text{crit}}} \right), \quad (8)$$

where  $t_0 = 100 \text{ years}$  and  $\rho_{\text{crit}} = 6.6 \times 10^{-12} \text{ g cm}^{-3}$  (cf. Nayakshin 2010c). The latter density value is the mean embryo density at inception for an embryo of 10 Jupiter masses (cf. eq 11 in Nayakshin 2010c). This prescription reproduces the correct limit for optically thick embryos (although the constant in front does change with  $\kappa_0$ ). For low density gas the cooling time is suitably short, so that we find that such gas is isothermal unless it is shocked (e.g., Fig. 4). Most importantly, it reproduces the widely accepted fact that protostellar discs cannot fragment in the inner  $\sim 50 \text{ AU}$  but may well fragment at larger distances if there is a sufficient mass of gas (Gammie 2001; Rafikov 2005; Rice et al. 2005; Meru & Bate 2010; Boley & Durisen 2010).

The central star is represented by a sink particle with an accretion radius of 1 AU. Both gas and dust particles arriving within this radius from the star are accreted.

### 2.5 Initial conditions and early evolution

We start with a gas disc of mass  $M_d = 0.4 M_{\odot}$  in a circular rotation around the star with mass  $M_* = 0.6 M_{\odot}$ . The disc inner and outer radii are 20 and 160 AU, respectively, and the disc surface density profile follows  $\Sigma(R) \propto 1/R^2$  law. At a given radius  $R$ , the disc initially has a constant density and the vertical scale height is  $H = R(M_d/M_*)$ . The initial circular rotation velocity curve is corrected for the disc mass interior to each point to avoid initial strong radial oscillations of the disc, but not for the gas pressure gradient force. Once the simulation starts, we find that gas temperature evolves quickly due to cooling and the compressional heat, and hence any initially imposed pressure profile erodes rapidly. Boley et al. (2010) used a similar setup and encountered a similar ‘‘difficulty’’ with their initial conditions. We note that a better approach to setting the initial condition is not a better relaxed gaseous disc but rather a more fundamental approach where the disc forms self-consistently, such as in the 2D simulations by Vorobyov & Basu (2005, 2006, 2010). We plan to present results of simulations initialised in a similar fashion in future papers. Nonetheless, our present study is valuable in itself as it shows that the ‘‘burst mode’’ of protostar accretion may arise in isolated star plus disc systems provided that the disc mass is sufficiently high.

The initial number of SPH particles is  $N_{\text{sph}} = 10^6$ , and half that for dust particles. The total number of particles is therefore  $1.5 \times 10^6$ . The initial grain size is  $a = 0.1 \text{ cm}$  for all the grain particles, and the total mass of the grains is 0.01 times the disc gas mass. Note that grains of sizes much smaller than this grow rapidly by sticking with small grains due to Brownian motion of the latter (Dullemond & Dominik 2005), therefore we neglect that phase of the grain growth.

### 3 RESULTS: GAS DYNAMICS

Gas is the dominant component in the disc, and its evolution affects the dust component greatly. Therefore we begin by discussing the behaviour of the gaseous component only, with the dust analysed later on.

#### 3.1 Fragmentation of disc onto clumps

Figure 1 shows several snapshots of the gas surface density from the simulation. The earliest one of the snapshots shown (the panel in the left upper corner) corresponds to time  $t = 2320$  years; all the following ones are separated by a time interval of 120 years, and follow from left to right, from top to bottom. The right most panel on the bottom is thus at time  $t = 3280$  years. The spatial extent of the box in the panel is from  $-230$  to  $230$  AU in both horizontal and vertical directions. The colour in the panels shows the gas column density, with black colour corresponding to  $0.05 \text{ g cm}^{-2}$  and the yellow showing the maximum set at  $\Sigma = 2 \times 10^4 \text{ g cm}^{-2}$ . The panels are centred on the star, whose position is not fixed in space and of course varies with time due to disc and gas clump gravitational forces.

Analysing gas dynamics now, we note that, released from the initial condition, the disc contracts vertically and achieves high midplane densities. As a result the disc becomes gravitationally unstable and forms spiral features in the inner disc regions first, since dynamical time is shortest there. As the disc is very massive, there are only two spiral “arms”. Also, there is apparently a radial mode in the instability as well, as one notes a broken nearly ring-like structure separating the outer and the inner disc regions. This is possibly due to the initial disc not being in an exact radial pressure-force equilibrium (see §2.5) as it is rapidly evolving.

Already in the second panel (middle top one) we observe formation of dense gaseous clumps inside the dense filaments (or arms) in the disc. Most clumps appear to interact strongly with their neighbours which is expected based on analytical arguments of Levin (2007) for gas clumps in an AGN disc (his arguments are local and hence scale free).

Note that the closest distance to the parent star where the clumps are born is about 70 AU, which is commensurate with previous analytical and numerical work by a number of authors, indirectly confirming that the radiative cooling prescription used in our simulations is reasonable. As time progresses, clumps are born also at larger radii, out to about 150 AU or so.

Clumps interact strongly with each other and also the surrounding gas. Both gas and the clump populations spread radially in either direction. This is apparent from comparison of the top and the bottom panels of Figure 1.

#### 3.2 The two phases of the disc

Figure 1 shows that the originally strongly unstable disc divides into two distinct phases or populations: the clumps and the “ambient” disc. The physical distinction here is that the clumps are self-gravitating whereas the disc material is marginally if at all self-gravitating. The exact division of the gas onto these two phases is definition-dependent and thus somewhat arbitrary, but we suggest two ways to do this that

we feel are reasonably meaningful and robust. Both of these are based on the local gas density,  $\rho$ .

The simplest one is to say that gas above some critical density belongs to the clump population and that gas with a lower density belongs to the disc. A suitable choice for the critical density is  $\rho_{\text{crit}}$  in the radiative cooling prescription (Eq. 8). To be more quantitative, we define a cumulative distribution function of SPH particles over different gas densities,  $f_\rho(\rho)$ , defined as the mass fraction of gas with density smaller than  $\rho$ . By definition,  $f_\rho(0) = 0$  and  $f_\rho(\infty) = 1$ .

This definition makes most sense when studying the densest end of the gas distribution function, as we find no gas significantly denser than  $\rho_{\text{crit}}$  outside the gas clumps except in the inner disc, at  $R \lesssim 10$  AU or so. Another useful, and potentially more discriminating, way to ascribe the gas to one of the two populations is to compare the gas density to the local tidal density,  $\rho_{\text{tid}}$ ,

$$\rho_{\text{tid}} = \frac{M_\star}{2\pi R^3}. \quad (9)$$

A marginally self-gravitating disc maintains vertically averaged gas density  $\rho \approx \rho_{\text{tid}}$  (cf. Goodman 2003); therefore the gas with  $\rho \gtrsim \rho_{\text{tid}}$  may be said to belong to the clumps *or perhaps* to spiral arms or filaments, whereas gas with  $\rho \lesssim \rho_{\text{tid}}$  belongs to the non self-gravitating component of the disc. We note that it is entirely possible for some SPH particles to cross from one population into the other and back, as behaviour of the disc is highly dynamic and the high density features may appear and later dissipate.

For a more detailed analysis a function  $F_\rho(x)$  is introduced in analogy to  $f_\rho(\rho)$  as a fraction of gas whose density is smaller than a given fraction  $x$  of the tidal density, e.g., satisfying  $\rho/\rho_{\text{tid}} < x$ .

Figure 2 shows the two cumulative gas density distribution functions for several different times, from  $t = 1800$  years (solid) to  $t = 5400$  years (dot-dashed). The left panel of the Figure shows that as time goes on, the maximum gas density increases, which physically corresponds to gas clumps contracting with time. The right panel of the Figure demonstrates this even more vividly, showing almost a step-function change for  $F_\rho$  at  $\rho/\rho_{\text{tid}} \approx 1$ . This tells us that gas divides very clearly into two distinct phases – the clumps and a non-self-gravitating component. Confirming that the “ambient disc” is indeed not self-gravitating at later time is the fact that there are no significant spiral features then (cf. Figure 8 for example).

Figure 3 shows the evolution of the mass in the two disc phases with time. In particular, the red line shows the mass of the gas that has density less than 10 times the local tidal density,  $\rho < 10\rho_{\text{tid}}$ ; the black curve shows gas that is at least moderately gravitationally-contracted, with  $\rho > \rho_{\text{tid}}$ , and the green one shows a strongly bound component with  $\rho > 10\rho_{\text{tid}}$ . By definition, the green and the red together amount to the total gas mass, i.e.,  $0.4 M_\odot$  minus gas accreted by the star at any given time.

Analysing Figure 3, we recall that early on there is an initial condition relaxation phase. As initially there is no dense and bound gas clumps, there is also no gas exceeding 10 times the local tidal density, and the red curve thus accounts for all the gas mass initially. Later on, spiral density features form in the disc. The black curve increases to encompass as much as  $0.3 M_\odot$  of material at time slightly

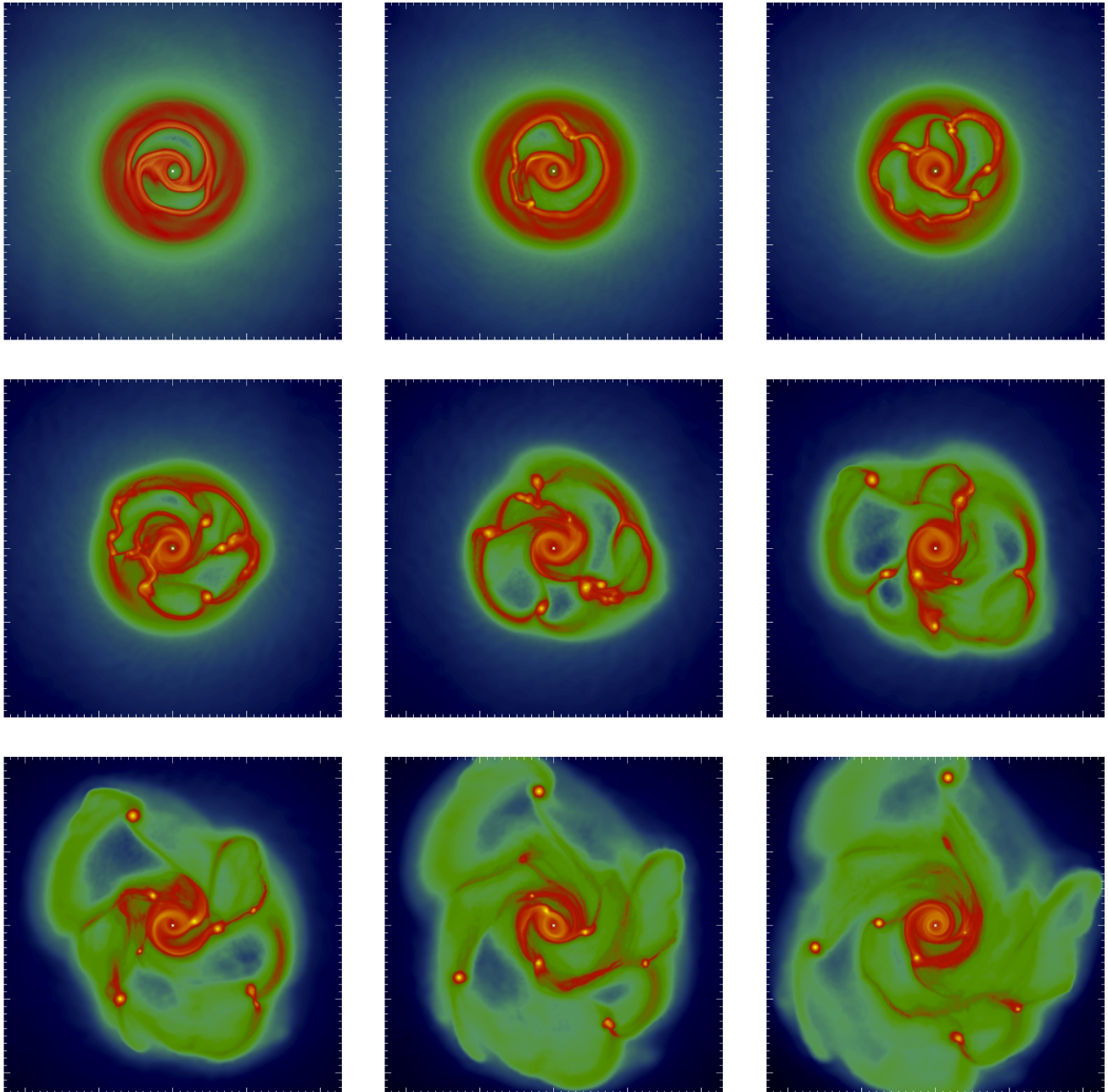


**Figure 1.** The evolution of the gas surface density profile in the simulation for several snapshots, starting from time  $t = 2320$  years (upper left) to  $t = 3280$  years (lower right panel). The box size is 460 AU on a side, and the colours indicate surface density from  $0.05 \text{ g cm}^{-2}$  (black) to the yellow,  $\Sigma = 2 \times 10^4 \text{ g cm}^{-2}$ . Note the radial migration and disruption of several clumps some  $\sim 30$  AU from the star.

after 2000 years. Most of that gas is weakly bound, as the mass in the green curve component is small at that time.

What is interesting is an ensuing rapid fall in that mass: by about 3000 years the marginally self-gravitating gas accounts for only  $\sim 0.17 M_{\odot}$  of the material. At the same time, the strongly bound component, clearly corresponding to the clumps, increases sharply to about  $0.13 M_{\odot}$ . Taken together it means that most of the gas is in either one of the phases – either the tightly bound clumps containing about a third of the total mass, or the non-self-gravitating part.

Indeed, the moderately bound material in the middle, with  $\rho_{\text{tid}} < \rho < 10\rho_{\text{tid}}$ , corresponds to the difference between the black and the green curves, and that amounts to only  $\sim 0.05 M_{\odot}$  of gas, e.g., slightly more than about 10% of the disc mass after  $t \sim 3500$  years.

There are two periods when the green curve decreases with time in Figure 3, whereas the red curve correspondingly increases. These time periods correspond to times when the clumps are being tidally disrupted near the star, as we shall see later.

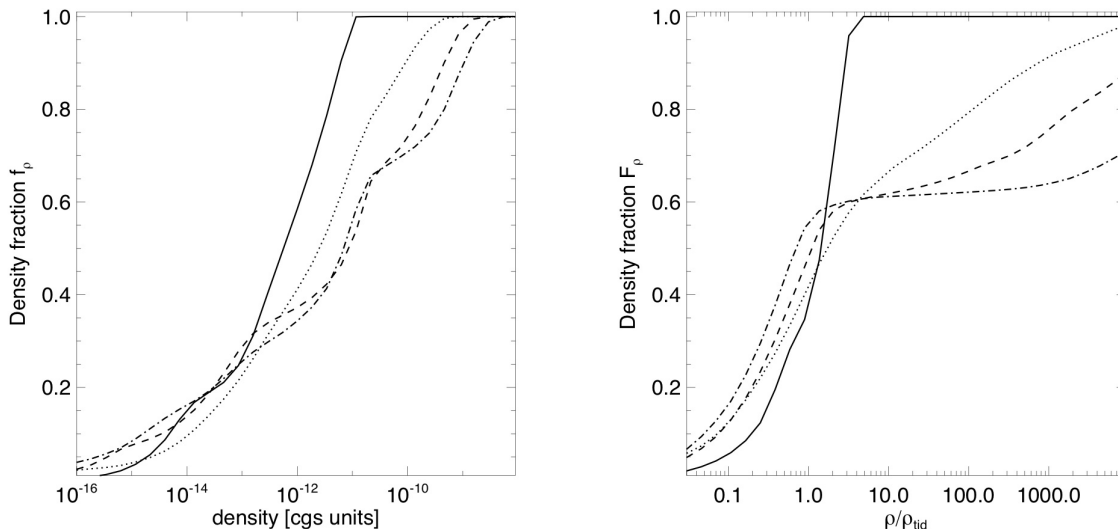


**Figure 2.** Cumulative density distribution functions  $f_\rho$  (left panel) and  $F_\rho$  (right panel) at times  $t = 1800, 3000, 4200$  and  $5400$  years for solid, dotted, dashed and dot-dashed curves, respectively. Both plots show that by later time, e.g.,  $t \gtrsim 3000$  years, about 40% of the gas resides in the high-density self-gravitating component, e.g., mainly the clumps.

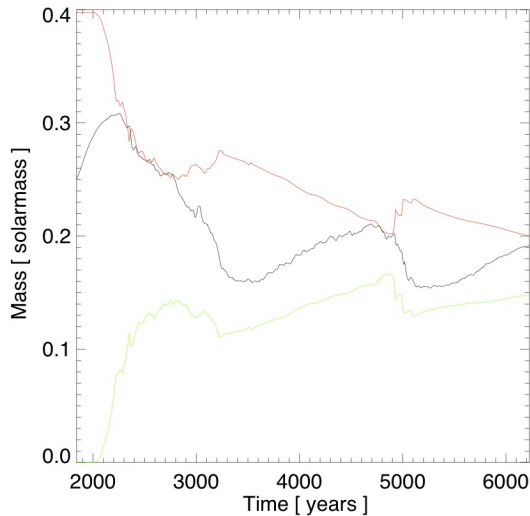


**Figure 3.** Decomposition of the gas by mass into the non self-gravitating component (red), mildly self-gravitating (black) and strongly bound (green) versus time. See §3.2 for detail.

### 3.3 Thermal structure of the disc

Figure 4 shows the gas column density together with velocity field (left) and the gas temperature (averaged over the respective column depth)  $t = 4880$  years. One notes that maximum gas temperatures are around 1000 K and are reached either in the inner disc (where our cooling prescription, designed to capture cooling of dense clumps, may underestimate cooling) or inside the gas clumps. There are also shocked gas regions that are heated to a few hundred K

typically. The gas density in those regions is relatively low, as comparison of the left and the right panels of the Figure shows. These shocked regions are most likely to be found in the space between the clumps or next to isolated clumps, where the “ambient” disc flow runs directly into the clumps (cf. the top left panel of Figure 5 for a higher resolution velocity field around the embryo).

The fact that the highest density regions are also the hottest in our simulations is crucial for setting the environmental conditions for grain growth. As grain growth is very strongly dependent on the surrounding gas density (see Eqs. 6 and §4.1), we see that grains that experienced growth are likely to have done so in a high temperature  $T \sim 1000$  K environments rather than in a cold-ish low density “ambient” disc. Of course embryos may be temperature-stratified, with cooler material on the outside of the embryos (e.g., Nayakshin 2010b), so that icy grains could still form in those regions, but the inner regions of embryos are able to melt and thermally reprocess even the most refractory species.

## 4 GRAIN GROWTH AND DYNAMICS

### 4.1 Grains grow inside embryos only

We now study grain growth and dynamics. Figure 5 zooms in on one of the densest embryos, the one closest to the star in Figure 4. The time of both figures is same,  $t = 4880$  years. Figure 5 shows the gas and the dust column densities (left top and left bottom, respectively), the gas temperature (right top) and the dust particle positions (right bottom; only half of the dust particles are plotted in the interest of better clarity of the figure). In the latter panel, dust particles of different grain size,  $a$ , are colour-coded as detailed below. The coordinate systems in both the spatial coordinates and in velocity space are centred on the densest part of the giant embryo for convenience.

The shape of the gas embryo is slightly elongated due to the tidal force along the  $x \approx y$  direction, which approximately coincides with the instantaneous direction to the star as one can see from Figure 4. The gas component rotates (spins) nearly as a solid body in the inner few AU of the embryo. The direction of rotation is prograde, i.e., same as that of the disc. This matches the earlier findings by Boley et al. (2010).

Comparing the dust and the gas column densities, there is clearly more than a passing resemblance of the two distributions. Note that even the velocity patterns, normalised on the largest velocity of the given component in the panel (thus slightly differently for the gas and the dust) are similar.

The colour coding in the right bottom panel of Figure 5 is as following:  $a < 0.5$  cm for the black dots,  $0.5 < a < 5$  cm for red,  $5 < a < 20$  cm for green, and  $20 \text{ cm} < a$  for blue. The approximate mass of these grain components is  $\sim 20, 27, 15$  and  $7.5 M_{\oplus}$ , respectively. The main point to note from this panel is the very concentrated and segregated dust distribution. The largest grains,  $a > 20$  cm are found exclusively in the very centre of the embryo, as a blue dot.

The concentration of the larger grains towards the centre of the gas embryo – the local potential well – is not unexpected. Since grains grow by hit-and-stick collisions in our model (Brownian motion is effective only for very small grains), e.g., two-body collisions, grains grow the fastest in a high density environment. Furthermore, the larger the grain the faster it sediments (Boss 1998).

This result is somewhat different from that of Boley & Durisen (2010) who considered grains of a fixed size spread evenly in their initial gas disc. Under these conditions the grains are concentrated to spiral arms and the clumps as well. In contrast, starting with small ( $a = 0.1$  cm) grains and making allowance for their growth, we find that grains grow a negligible amount everywhere except the planet embryos, e.g., even inside the initial spiral arms. To make this point more explicit, Figure 6 shows the grain size for the dust particles in the whole simulation domain versus density of the gas, defined on the SPH neighbours of the dust particles. Only a randomly selected fraction of dust particles is plotted for clarity of visualisation. There is nearly a one-to-one monotonic relation between the dust size and the density of the surrounding gas, splitting onto several nearly vertical “tails” at the right upper part of the Figure. This part of the diagram corresponds to several individual clumps.

The monotonic relation between the grain size and the gas density can be broken during periods of clump dispersal. During this time, the smaller grains move with the gas since they experience strong aerodynamic drag forces, so they are “frozen in” with the gas. However, the larger grains experience weak drag forces. Neglecting these weak forces, we can say that the large grains move under the influence of gravity only, whereas the gas experiences both the hydro and the gravity forces. Therefore, the larger grains can be actually separated from the gas due to the different forces that these components experience.

#### 4.2 Formation of a terrestrial planet core

Sinking of larger grains to the centre of a gas clump should eventually lead to the grain density in some region, called a

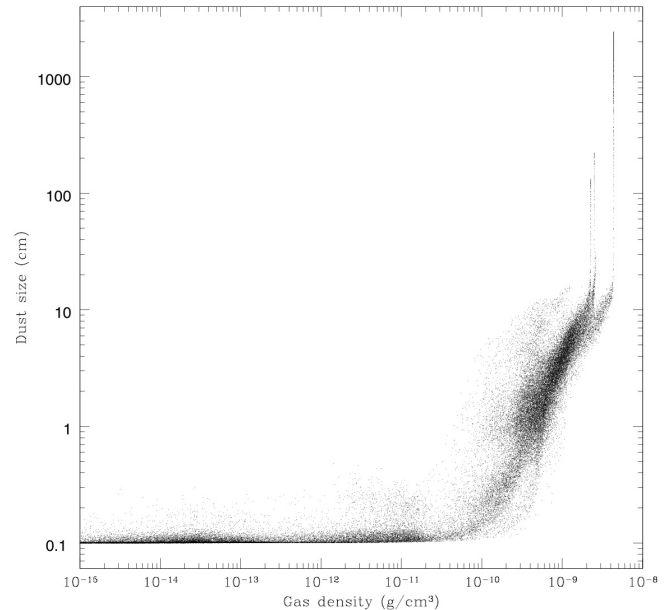


**Figure 6.** Grain size versus gas density at time  $t = 4880$  years. Dust growth can be seen to occur only in dense regions (e.g., clumps). Note the upward “tails” in the dust distribution on the right hand side of the plot, corresponding to dense dust cores in three different giant embryos. The densest “tail” at  $\rho_d \approx 5 \times 10^{-8} \text{ g cm}^{-3}$  corresponds to the “Super-Earth” clump.

“grain cluster” in Nayakshin (2010c), exceeding that of the gas, and then a gravitational collapse of the grains there. This is indeed what happens in the simulation. The panels in Figure 5 do not have the resolution required to discern this collapse. The blue “dot” in the lower right panel of the figure is actually a spatially compact cluster of grains numbering over 3000 dust particles. Had we not imposed the gravitational softening length of  $h_{\min} = 0.05$  AU (cf. §2), this cluster would have certainly collapsed, numerically speaking, to a point, and physically speaking to a terrestrial planet core.

Figure 7 shows the gas (black dots) and the dust grain density (color dots) inside the clump investigated in Figure 5. The colour scheme used for dust particles in Figure 7 is as following: red,  $a < 1$  cm; green,  $1 < a < 10$  cm; cyan,  $10 < a < 100$  cm; and dark blue,  $a > 100$  cm. There is a very clear segregation of grain particles by their size, as larger grains sink in more rapidly.

The gas density profile has the constant density shape in the inner part of the clump (cf. the purple curve in Figure 7), as expected for a polytropic gas cloud, and as found in 1D radiative hydrodynamics simulations by Nayakshin (2010c). The dust density is indeed higher than the gas density in the innermost 0.05 AU. We note that further evolution of the simulation shows that the dust particles in this innermost part of Figure 7 are self-gravitating and self-bound. When the gas component is disrupted (§5), the “grain cluster” survives the disruption and remains a point-like cluster of dust particles. As we argued in §2.3, the fact that we smooth out self-gravity of the dust particles but not the aerodynamic force or the stellar tidal force, which both oppose grain sed-



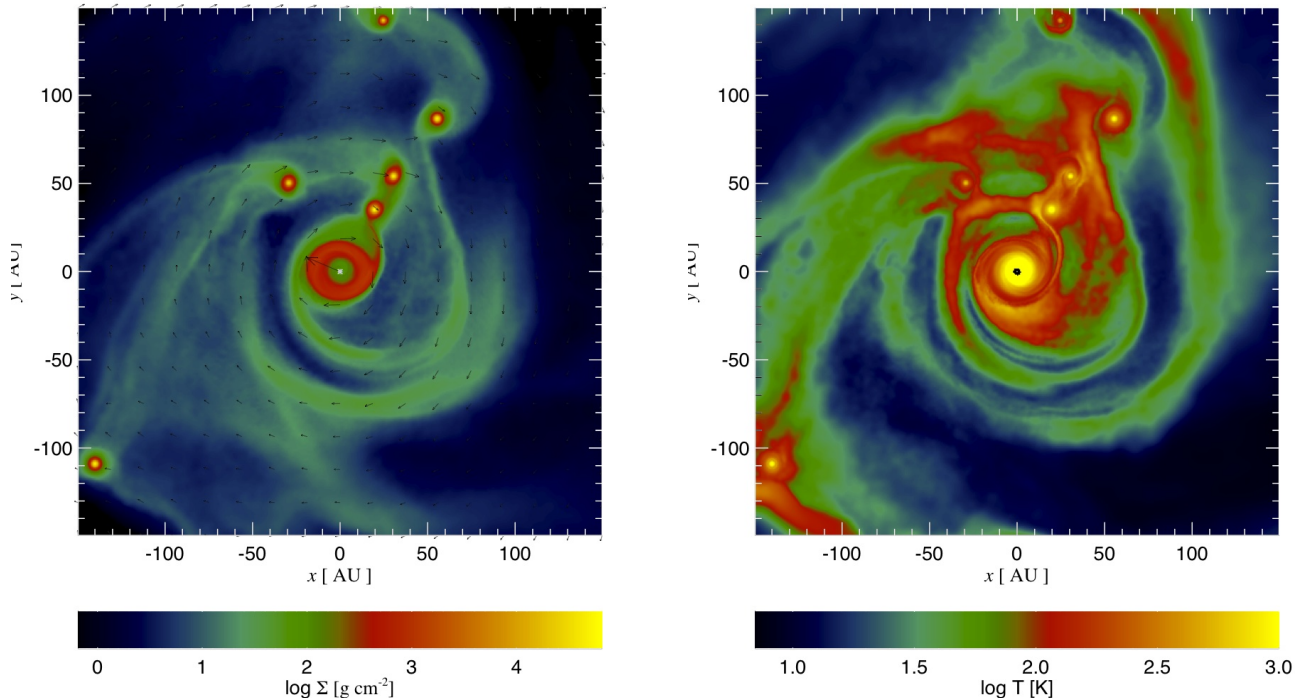


**Figure 4.** The column density (left) and the column-averaged temperature (right) of the gas at time  $t = 4880$  years. Note the clear division between the high density high temperature clumps, and the low density non self-gravitating regions, which may be cool or relatively hot due to shocks.

imentation, implies that the cluster would be even stronger self-bound in higher resolution (smaller gravitational softening value) simulations.

One could worry that due to the small physical size of the dust core, we somehow incorrectly estimate the gas density and hence the aerodynamic drag force between the grains and the gas in that region. However, the procedure for finding the SPH neighbours for dust particles is independent of the dust density or the dust concentration, as only the SPH neighbours are searched for. We checked that number of the gas neighbours for all the dust particles in Fig. 7 varies in the accepted limits, e.g., between 39 and 41. Therefore, the gas-density drag force does not “disappear” in the centre of the clump and we believe that the grain sedimentation in that region is entirely physical. Of course, due to a finite numerical resolution, we could miss some effects on smaller scales. For example, if the mass of the solids in this small scale region is very high, say 20 Earth masses, the gas itself could be influenced by the gravity of the dust particles (Nayakshin 2010b). The gas could then build-up to higher densities around the dust core. In the final disruption of the embryo some of this inner gas envelope could then survive. At this time we cannot resolve such small scales. However it would seem that these effects would make the solid core even more gravitationally bound, due to the increased gas mass in the region.

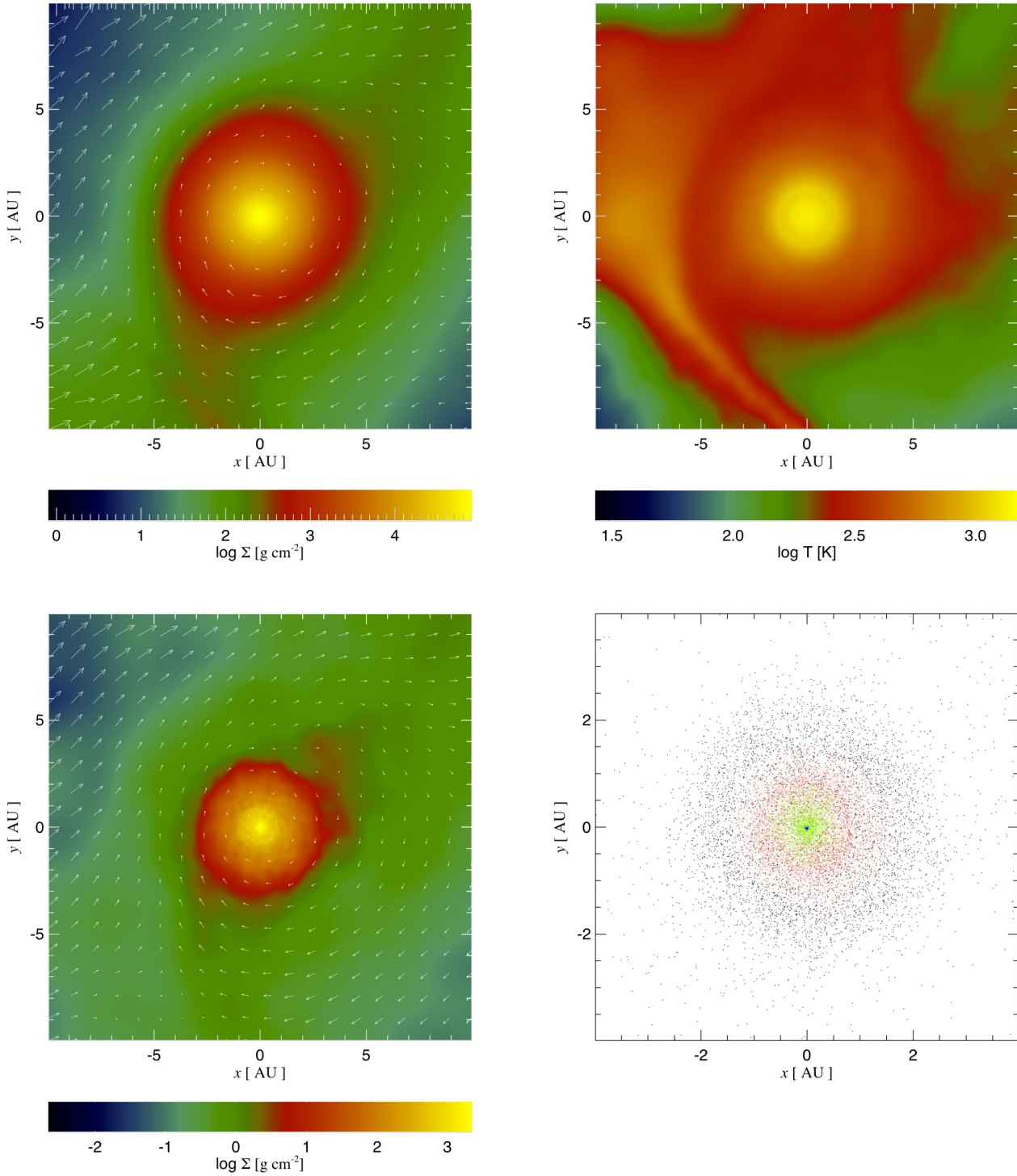
We also note that we do not find strong convective motions in our models that could resist smaller grain sedimentation. Future higher SPH particle number simulations will allow us to improve resolution at the smallest scales within the clumps. We also note that a better numerical treatment

of the problem should include proper radiation transfer, e.g., an account of the radiation emitted by the contracting solid core and then its propagation through the surrounding gas. We currently lack numerical capabilities for an explicit radiation transfer, both software and hardware wise (as a very high resolution is required near the centre of the embryo), but we plan to improve our methods in the future to address the “solid core” collapse to a numerical singularity better.

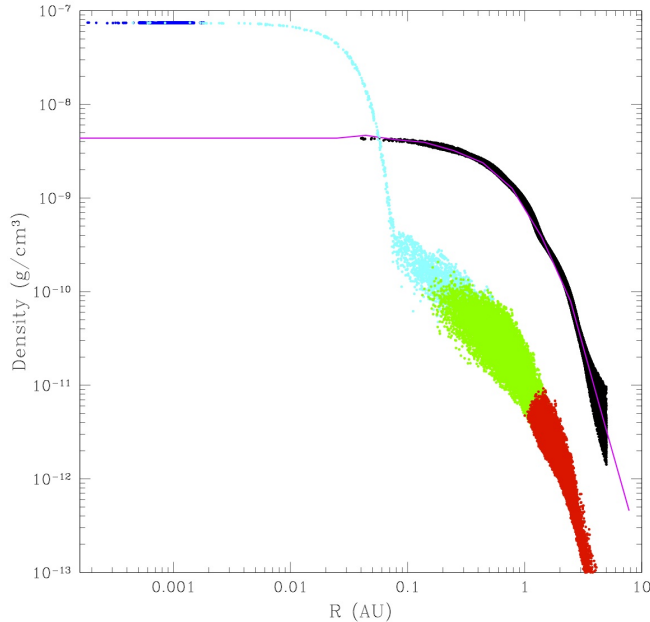
## 5 MAKING THE “SUPER-EARTH”

Figure 1 demonstrates a very dynamic and sometimes violent evolution of gaseous clumps. Clumps merge, some several times, with neighbouring ones. Close interactions may also result in velocity “kicks” to the clumps. The maximum kick velocity possible is a fraction of the sound speed in the clump, e.g.,  $\sim$  a  $\text{km s}^{-1}$  or so. The Keplerian velocity a distance  $R$  from the star is  $v_K \approx 2.3 R_{100\text{AU}}^{-1/2} \text{ km s}^{-1}$ . Therefore such interactions may result in substantial orbital changes for the clumps, as earlier suggested by Boley et al. (2010).

We now concentrate on the evolution of the clump investigated earlier in §4 and in Figures 5 and 7. This embryo forms on an initial orbit with the pericentre of  $\sim 70$  AU and the apocentre of  $\sim 100$  AU. The clump makes about three full revolutions around the star, interacting with nearby embryos. Remarkably, its last interaction with another passing embryo sinks it close enough to the star for it to be tidally disrupted. As pointed out in §4.2, the densest part of the dust particles inside the embryo (which we call a solid core below) is self-bound and is actually artificially kept from



**Figure 5.** The embryo closest to the star at time  $t = 4880$  years (cf. Figure 4). Gas (upper left panel) and dust (bottom left) column densities, with velocity fields, all centred on the densest point of the gas clump. The largest velocity vector in the upper left panel corresponds to velocity of  $6.2 \text{ km s}^{-1}$ , whereas the same for the lower left panel is  $3.9 \text{ km s}^{-1}$ . Gas temperature is shown in the upper right panel, and the lower right one shows grain particles positions with grains of different sizes marked by different colour as detailed in §4.1.



**Figure 7.** Dust and gas densities of clump “S” (see Fig. 8) at  $t = 4880$  yrs at the positions of the respective particles. The gas particles are shown with the black dots. The purple solid line shows spherically averaged gas density using logarithmic bins. Coloured dots show grain density at the positions of individual grain particles of different size: red is for  $a < 1$  cm, green for  $1 < a < 10$  cm, cyan for  $10 < a < 100$  cm and blue for  $a > 1$  m. Note a clear segregation of the grain particles, with the bigger ones found closer to the centre of the clump.

further collapse by the gravitational softening we employ on small scales. It is hence not surprising that the solid core survives the complete dispersal of the gaseous envelope and of the outer dust layers. The end result of this process is a terrestrial planet core, as earlier envisaged by Boley et al. (2010) and Nayakshin (2010a).

### 5.1 Dynamics of the Super-Earth embryo

Figure 8 shows several snapshots of the central 150 AU region near the star around the time immediately preceding the embryo disruption. The order of the snapshots is from top to bottom, left to right. The first one and the last one corresponds to times  $t \approx 4680$  years and  $\approx 5000$  years, respectively. Concentrating on the innermost  $\sim 70$  AU of the Figure, one notes the close interaction between the closest (marked as “S”) and the second closest (marked 1 on the Figure) to the star gas clumps. The two happen to be separated by about 20 AU for a quarter or so of a rotation (see the middle row of panel in the figure) for the innermost clump, whose orbit is only slightly eccentric before the interaction. As a result of the second embryo being positioned behind the first one during this interaction, the first one appears to loose angular momentum to the second. After the interaction the innermost one is thrust inwards on a much more eccentric orbit with a pericentre of about 10 AU, whereas the other clump is sent on a wider orbit. The

innermost clump is subsequently disrupted and is dissolved inside the innermost disc.

We shall now refer back to Figure 3 and note that there is a significant depression in the curve of the total masses of both the strongly bound gas component (the green curve) and the mildly bound one as well (the black curve) at around time  $t \approx 5000$  years. We now see that this event corresponds to the destruction of the innermost embryo by the tidal field of the star. The total mass of the embryo is  $\sim 25 - 50$  Jupiter masses, depending on where one puts the embryo outer boundary. There is an associated increase in the non self-gravitating gas component (the red curve), followed by a slower decline. The decline in that curve is mainly due to accretion of gas onto the star. We note that the clump inward migration and destruction we found here is of course related to the results of Vorobyov & Basu (2005, 2006, 2010).

### 5.2 Clump disruption: gas dynamics

Expressing the tidal density in terms of numerical values,

$$\rho_{\text{tid}} = \frac{M_*}{2\pi R^3} \approx 6 \times 10^{-11} \text{ g cm}^{-3} \left( \frac{10 \text{ AU}}{R} \right)^3. \quad (10)$$

Given the outer regions of the gas clump have density of a few  $\times 10^{-12} \text{ g cm}^{-3}$ , we see that these outer regions can be tidally stripped at a distance of 20-30 AU from the star, at which point  $\rho \sim \rho_{\text{tid}}$ .

The flow of the gas at earlier disruption phases can be seen in the last three panels of Figure 8. Figure 9 shows the inner part of the disc and what is left of the disrupted embryo at time  $t = 5080$  years. Overlaid on the gas density plot are the velocity vectors, and also some of the dust particles. The black square shaped symbol, marked with the label “SE”, at  $(x, y) \approx (2, 11)$  shows the only surviving part of the dust core. The core, defined as a very compact ( $R \lesssim 0.01$  AU) concentration of about 3000 dust particles with  $a \gtrsim 50$  cm, has a mass of about  $7.5M_{\oplus}$ . As explained earlier, this core should physically be considered to be a terrestrial-like planetary core of the “Super-Earth” mass range.

### 5.3 Clump disruption: dynamics of solids

Here we concentrate on the dynamics of the dust particles from and around the “Super-Earth” clump. The object circles the star on a small eccentricity ( $e \sim 0.1$ ) orbit with the semi-major axis of about 8 AU until the end of the simulation.

Smaller dust particles are unbound (tidally disrupted) during the clump destruction. The cyan points in Figure 9 show some of the “small” dust particles, with size  $a$  between 1 and 2 cm. These smaller particles were on the outskirts of the embryo (cf. Fig. 7), and are therefore easily disrupted from the embryo together with the associated gas. There is a leading and the trailing tail in these particles, as expected for a tidally disrupted object.

We shall now analyse the process of dust disruption in more detail. Figure 10 shows the dust-column averaged size of the grains at two specific times at the beginning of the embryo disruption,  $t = 4968$  years, and  $t = 5056$  years. The figure shows an effect that can be called “tidal segregation”. Namely, smaller grains are stronger bound to the gas (e.g., Weidenschilling 1977) and are also predominantly found in

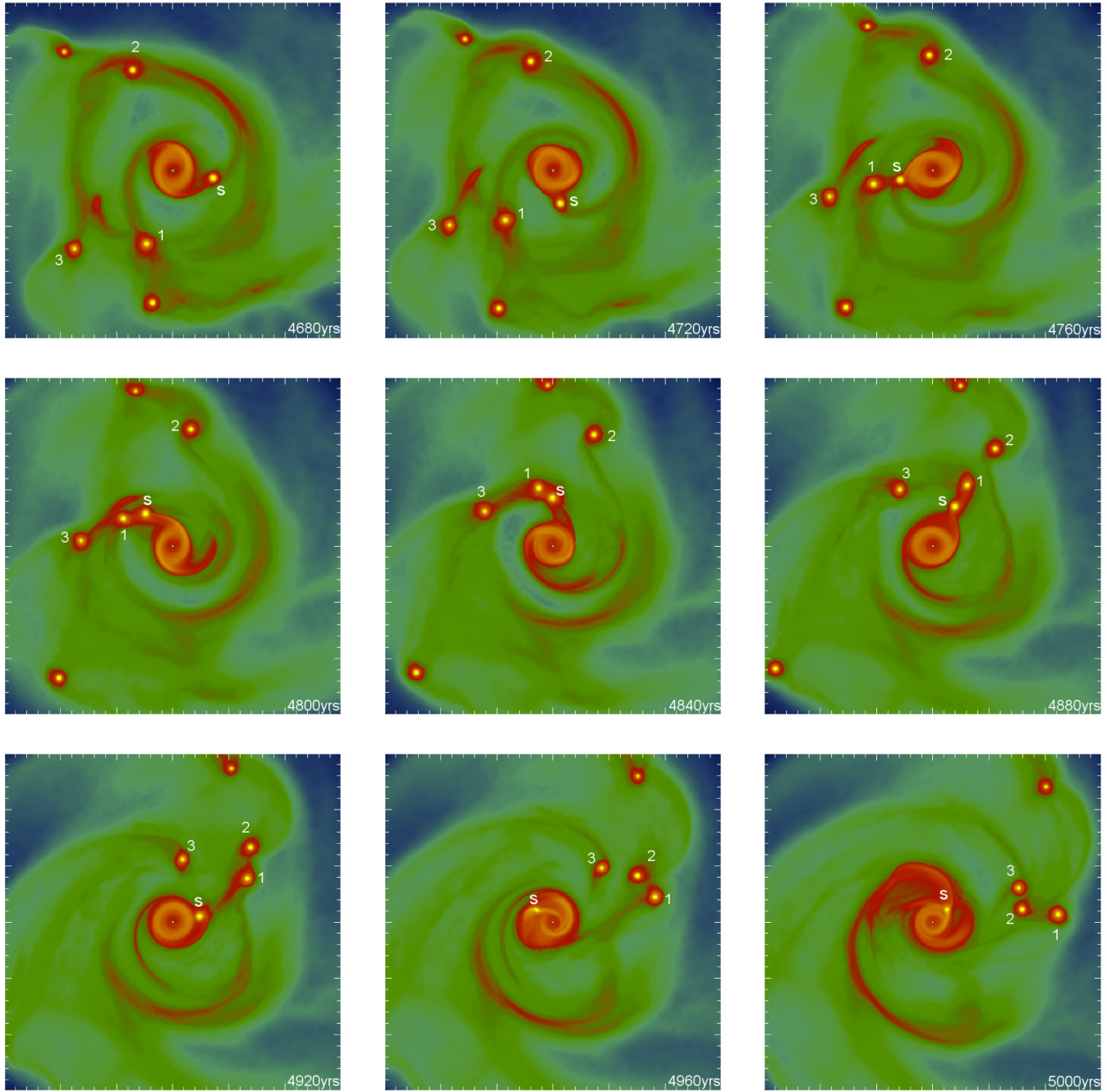


**Figure 8.** Snapshots of the gas surface density profile in the inner 150 AU (each box is 300 AU on a side), at nine different times, starting from  $t \approx 4680$  years (upper left) to  $\approx 5000$  years (bottom right). The consecutive frames are separated by 40 years. The color scheme is same as in Figure 1. The gas clump closest to the star (marked “S” for the “Super-Earth”) loses angular momentum to another clump (numbered as 1 in the panels) in a close interaction, and plunges closer in to the star. This leads to a very rapid tidal mass loss through both inner and outer Lagrange points, eventually leading to a complete embryo dispersal and incorporation into the ambient gas flow.

the outer reaches of the embryo (cf. Figures 5 and 7). Therefore, as the gas clump is disrupted, the smaller grains are the first to be stripped away. For example, only  $a \lesssim 1$  cm grains are unbound from the clump in the left panel of Figure 10. In the right panel, however, the tidal disruption spreads to more inner regions of the embryo and we have grains of  $a \sim$  tens of cm spread into the narrow leading and trailing dust filaments. The Super-Earth core survives, however, as its

density is around  $10^{-7} \text{ g cm}^{-3}$  (cf. Figure 7), i.e., orders of magnitude higher than the tidal density at this location. The solid core is visible as a bright yellow dot in both panels. Note that the dimensions of the dot in the Figure are given by the size of a pixel, which is much larger than the physical size of the Super-Earth core (see below).

At later times all of the gas and all the intermediate size grains are disrupted from the embryo. Figure 11 shows

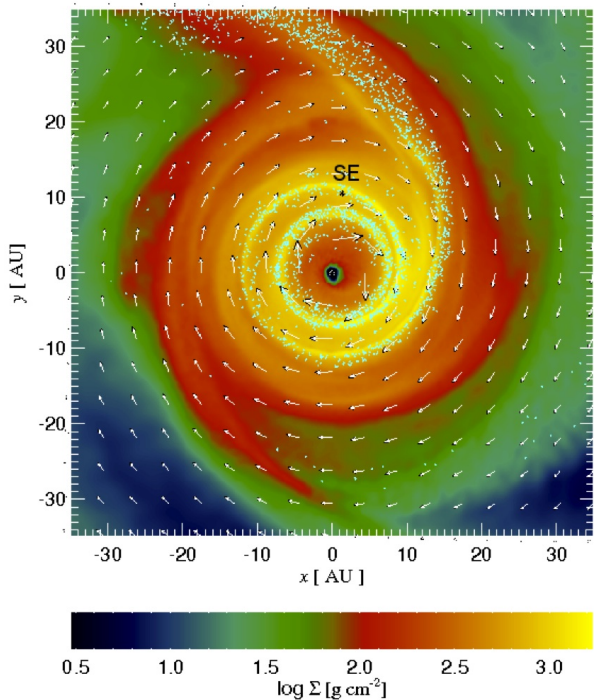


**Figure 9.** The gas column density with velocity vectors and some of the dust particles. The Super-Earth is the black symbol approximately north of the star.

grain size maps analogous to Figure 10 but on smaller spatial scales. The Super-Earth core is now “all alone”, with smaller dust particles significantly influenced by the drag forces from the disc. The right panel of Figure 11 demonstrates that larger grains  $a \gtrsim$  tens of cm are lost into the star more rapidly than smaller  $\sim 1$  cm grains. The Super-Earth ends up on a slightly eccentric orbit with eccentricity of about 0.1 and a semi-major axis of  $\approx 8$  AU.

Figure 12 concentrates on dust particles within  $R \sim 3$  AU from the Super-Earth core for several different times around the gas clump disruption, as labelled on the Figure. The Figure shows the radial velocity (defined with respect to the velocity of the Super-Earth) of dust particles as a function of distance from the core. The particles of different size are shown with different colors, following the color convention of Figure 7. As we under-estimate (smooth) gravitational forces on small scales, particles found within 0.01 AU from the centre of the dust core, defined as its densest point, are collectively shown with a thick blue dot. The number of dust particles within the dot is shown with in the lower left corner of each panel.

Before the tidal disruption of the core, the radial velocities of dust particles are small everywhere except outside the inner couple AUs, where the dust may be influenced by external gas velocity field. This is expected as dust sedimentation velocities are quite small Boss (1998); Nayakshin (2010b). Starting from the second panel from the top ( $t = 4960$  yrs), dust radial velocities increase (note the increased vertical scale on the velocity axis).

The disruption of the gas embryo affects the dust particles within in two ways. Firstly, the mass enclosed within

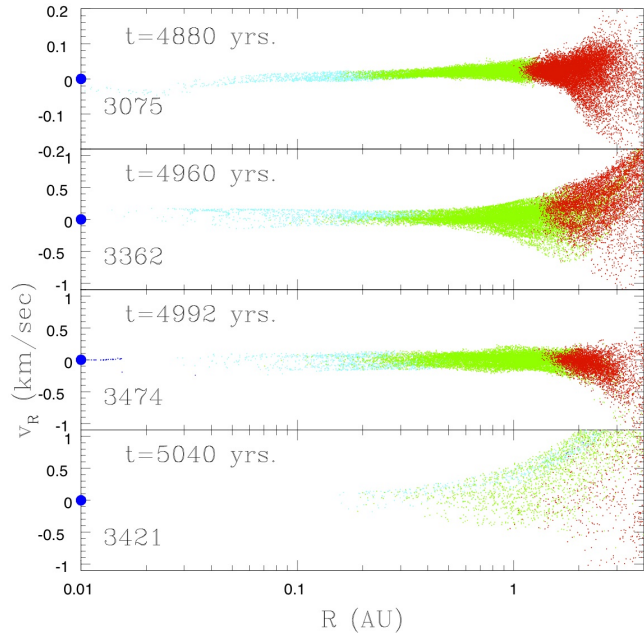


**Figure 12.** The radial velocity of dust particles inside the clump around the disruption time. The colors coding of the grain sizes is the same as in Fig. 7. The large blue dot at  $R = 0.01$  AU represents the “Super-Earth” core composed of the large grains ( $> 1$  m). The numbers in the left lower corners of the panels show the number of dust particles within the 0.01 AU (represented by the blue dot). Note that all the smaller particles (cyan, green and red) are eventually stripped away from the Super-Earth core.

a given radius decreases, reducing the gravitational attractive force on the dust. Secondly, gas outflowing away from the centre of the clump applies aerodynamical drag forces on the dust. This strips away all but the largest  $a > 100$  cm particles. In the last panel of Figure 12, the Super-Earth core is a stand-alone feature. We note that the mass of the core slightly decreases between the third and the fourth panels of the Figure, which indicates that some  $a > 100$  cm particles are also dispersed by the tidal disruption. However, as we soften the self-gravity of the dust within 0.05 AU (cf. section 2), better resolved numerical simulations could have resisted even this slight mass loss of the core. Finally, we note that the mass of the Super-Earth stabilises and does not decrease at later times.

## 6 DISCUSSION

We presented a 3D numerical simulation of a massive gas disc with the usual interstellar mass fraction of dust grains. The grains are treated as a second fluid interacting gravitationally and via gas-drag friction with the gas. The size of the grains is allowed to grow with time by grain-grain collisions. We used a simple density-dependent radiative cooling time prescription allowing the gas to cool rapidly at low densities and increasing the cooling time at higher densities, as found for spherical gas clumps (Nayakshin 2010c). The simulation was selected from a set of  $\sim 10$  of similar simulations

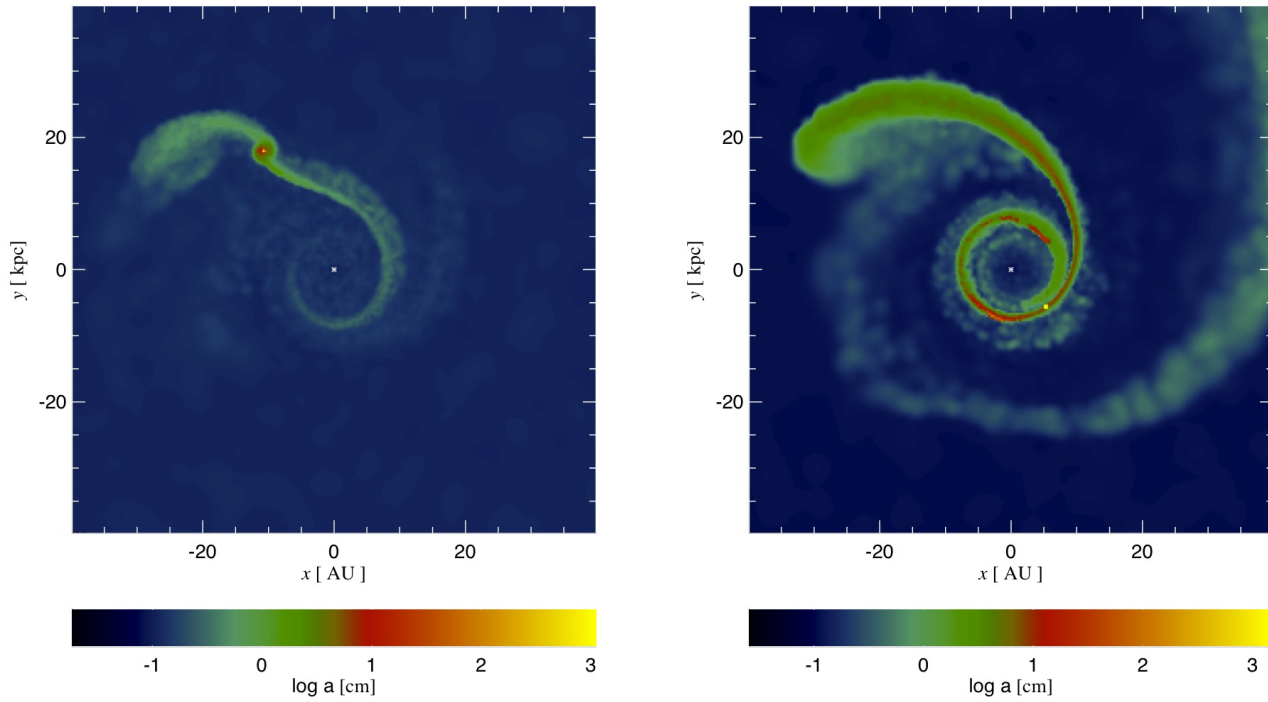


**Figure 10.** Grain size at two different times in the beginning of the clump disruption. Left panel has  $t = 4968$  years, and the right one corresponds to  $t = 5056$  years. Note that the largest grains are all in the point-like core that is resistant to tidal shear, whereas the smaller grains are being sheared away. The smaller the grains the earlier they are sheared away from the embryo.

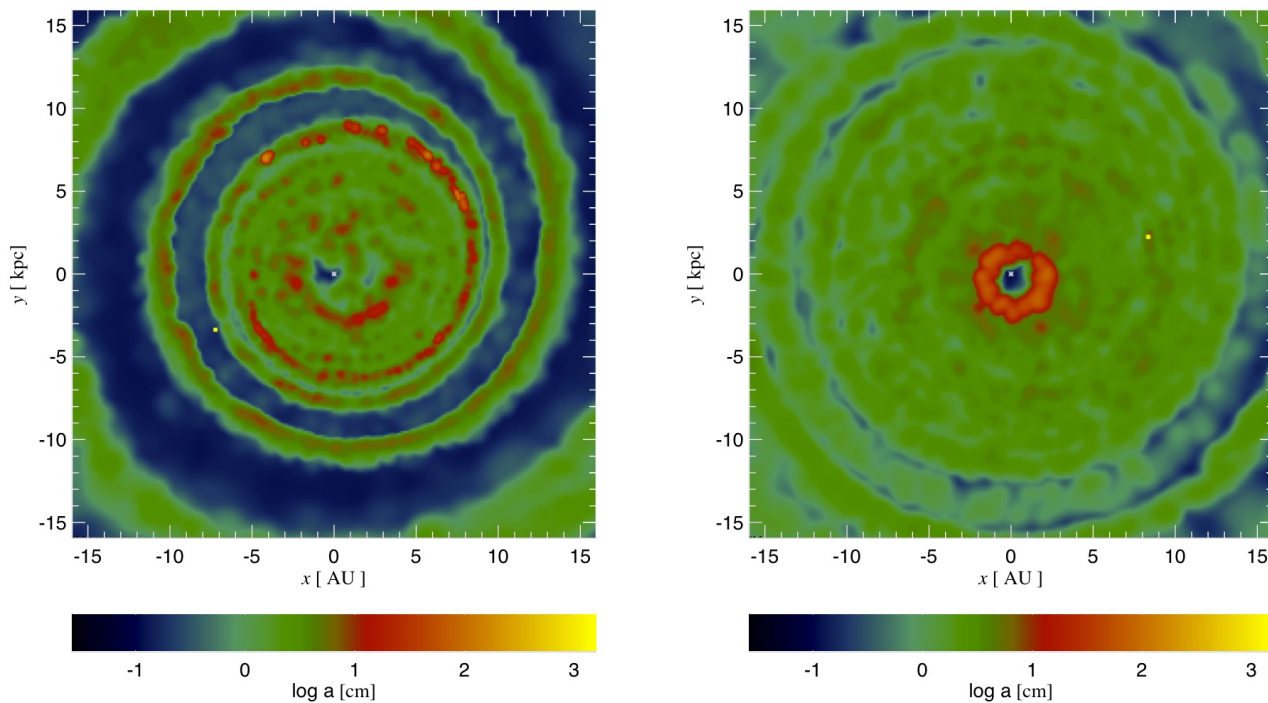


**Figure 11.** Same as Figure 10 but at later times,  $t = 5136$  and  $t = 5360$  years, respectively. Note also the smaller spatial scale. The “Super-Earth” core is the bright yellow dot on orbit with eccentricity  $e \approx 0.1$  and semi-major axis of about 8 AU.

with varying initial conditions and/or cooling prescription (more on this below).

While not presenting the results of the other simulations performed, we note that all of them showed the following results, exemplified by the simulation presented here: (a) Spiral arms arising in the disc fragment into clumps at large radii due to the cooling time becoming longer than the local dynamical time at high densities. (b) The clumps do interact with each other, strongly affecting their orbits. The orbits of clumps may be eccentric due to clump-clump interactions (see also Boley et al. 2010). (c) Bodily interactions of clumps usually result in mergers, although dispersal of the clumps may occur if the relative angular momentum of the clumps is too large. (d) As earlier found by Vorobyov and Basu (Vorobyov & Basu 2005, 2006, 2010), inward migration of clumps is quite generic, and in the presence of many clumps may not easily be analytically described. (e) Some clumps may remain far out, e.g.,  $\sim 100 - 200$  AU for the initial disc size of 200 AU, again consistent with Vorobyov & Basu (2010). (f) The initial inventory of gas divides onto two physically distinct components at later times – the high density strongly self-gravitationally bound clumps, containing about 40% of the material in the simulation presented here, and the “ambient” non self-gravitating gas disc with density below the local tidal density. No strong spiral arm features remain in the disc at late times, except in the inner 20 AU or so. (g) Within the simulation time of  $\sim 5000$  years, grain growth occurs only inside the high density gas clumps. This is not surprising as the hit-and-stick grain growth rate is proportional to density, and the density in the clumps is several orders of magnitude higher than in the ambient disc.

The final fate of the clumps and thus the outcome of the simulation in its entirety does depend on the cooling prescription (as also expected based on analytical models of Nayakshin 2010c,b,a), initial conditions, e.g., the disc mass, and missing physics (e.g., exact radiative transfer, and a better opacity, dust growth and fragmentation models) not yet included into the code. If radiative cooling of clumps is not suppressed sufficiently strongly at high densities, they may cool and collapse into massive gas giant planets or low mass brown dwarfs (Stamatellos & Whitworth 2008). Inward migration of such objects would disrupt them only if they migrate very close to the star, e.g., sub-AU distances that we do not resolve in our simulations. On the other hand, if cooling is suppressed too strongly at high densities, the gas clumps are found to be too fluffy and are disrupted at 30-40 AU. There is a further constraint on the planet formation part of our simulations. Grain growth needs to be rapid enough to result in a terrestrial planet core by the time the embryo is tidally disrupted, or else the grains are disrupted as well, and presumably accreted by the star.

The simulation presented in the paper was selected because it did result in one rocky-core bearing embryo being delivered into the inner disc and being disrupted there. Therefore, as stated in the Introduction, the simulation presented here is only a “proof of the concept”: the tidal downsizing hypothesis *may* work. Further surveys of the parameter space, improvements in the simulations, both in terms of numerical resolution and especially the missing physics are needed to understand how robust the tidal downsizing route for planet formation might be.

In addition, our simulations spanned  $10^4$  years at the

most due to numerical expense of the calculations. We expect that on longer time scales the behaviour of the system may change considerably. At lower disc masses the disc may become only marginally unstable in the sense of bearing spiral arms but not giving birth to high density clumps we concentrated upon here. It is therefore possible that on longer time scales, e.g., millions of years, dust would grow within the spiral arms as well (e.g., Clarke & Lodato 2009; Boley & Durisen 2010). Further migration of planets born in the early massive disc phase might be expected in this case.

One somewhat surprising result was to find that clumps were usually disrupted at greater distances (typically 20-30 AU) than expected based on the analytical theory of Nayakshin (2010a). This may indicate that clumps embedded in a massive and rapidly evolved disc are “harassed” by their environment and are thus less compact than similar isolated clumps. Rotation of the embryos, not taken into account in analytical models of Nayakshin (2010a) may be another mechanism providing support against gravitational contraction of the gas clumps. Alternatively the simulation results may also mean that clumps are disrupted at densities much lower than the mean embryo density as assumed by Nayakshin (2010a). We plan to investigate these issues more fully in future work.

Another, not unexpected, result is that clumps formed at different parts of the disc evolve differently. The clumps formed the closest (and earliest) migrate inward too rapidly for their grains to grow large enough for a dense core formation. In the simulation presented, there are two earlier clump disruption episodes each of which did not contain a sufficiently dense grain core to survive the disruption. There are also partial disruption events when gas clumps would lose only a part of their mass and then “hang around” at a slightly wider orbit. This indicates that even if the physics of embryo cooling and dust growth and sedimentation are fixed, there is still a broad scope for different outcomes. The result of planet formation in the tidal downsizing hypothesis may thus be quite varied if embryo-embryo interactions are important and frequent.

Concerning the missing physics, we believe that energy release by the collapsing massive dust cores is the most consequential. As found by Nayakshin (2010b), and argued much earlier by Handbury & Williams (1975), these cores may release so much binding energy as to remove most of the outer hydrogen-rich envelope even *without* tidal stripping, perhaps resulting in icy giant planets at relatively large separations, where they could not have possibly been affected by tidal forces of the star. This would require introducing a proper radiative transfer in the simulations. Irradiation from the parent star is another significant effect missing from our work. We plan to include at least some of this physics into our future work and also cover a broader set of parameter space and initial conditions.

## 7 CONCLUSIONS

We presented one “proof of the concept” simulation (selected from about a dozen) that produced a massive enough giant planet embryo to have migrated to within about 10 AU of the parent star. This embryo is dense enough and aged enough to allow grains a sufficient time to grow and sed-

iment to its centre. Future simulations of this kind should include more of the relevant physical processes and sample a broader range of initial conditions and the parameter space to indicate whether such embryo migration and tidal disruption are common enough to explain the abundance and properties of the observed planets.

## 8 ACKNOWLEDGMENTS

Theoretical astrophysics research at the University of Leicester is supported by a STFC Rolling grant. We thank the anonymous referee for their contribution to improving this paper.

## REFERENCES

- Baraffe I., Chabrier G., Barman T., 2010, Reports on Progress in Physics, 73, 1, 016901
- Bate M. R., Bonnell I. A., Bromm V., 2003, MNRAS, 339, 577
- Blum J., Wurm G., 2008, ARA&A, 46, 21
- Boley A. C., 2009, ApJL, 695, L53
- Boley A. C., Durisen R. H., 2010, ArXiv e-prints
- Boley A. C., Hayfield T., Mayer L., Durisen R. H., 2010, Icarus, 207, 509
- Boss A. P., 1997, Science, 276, 1836
- Boss A. P., 1998, ApJ, 503, 923
- Boss A. P., Wetherill G. W., Haghighipour N., 2002, Icarus, 156, 291
- Cameron A. G. W., 1978, Moon and Planets, 18, 5
- Cameron A. G. W., Decamp W. M., Bodenheimer P., 1982, Icarus, 49, 298
- Cassen P. M., Smith B. F., Miller R. H., Reynolds R. T., 1981, ICARUS, 48, 377
- Clarke C. J., Lodato G., 2009, MNRAS, 398, L6
- Cuzzi J. N., Hogan R. C., Shariff K., 2008, ApJ, 687, 1432
- Donnison J. R., Williams I. P., 1975, MNRAS, 172, 257
- Dullemond C. P., Dominik C., 2005, A&A, 434, 971
- Gammie C. F., 2001, ApJ, 553, 174
- Goldreich P., Tremaine S., 1980, ApJ, 241, 425
- Goldreich P., Ward W. R., 1973, ApJ, 183, 1051
- Goodman A. A., Benson P. J., Fuller G. A., Myers P. C., 1993, ApJ, 406, 528
- Goodman J., 2003, MNRAS, 339, 937
- Handbury M. J., Williams I. P., 1975, AP&SS, 38, 29
- Helled R., Podolak M., Kovetz A., 2008, Icarus, 195, 863
- Helled R., Schubert G., 2008, Icarus, 198, 156
- Johansen A., Oishi J. S., Low M., Klahr H., Henning T., Youdin A., 2007, Nature, 448, 1022
- Kuiper G. P., 1951, in 50th Anniversary of the Yerkes Observatory and Half a Century of Progress in Astrophysics, edited by J. A. Hynek, 357–+
- Larson R. B., 1969, MNRAS, 145, 271
- Levin Y., 2007, MNRAS, 374, 515
- Lin D. N. C., Bodenheimer P., Richardson D. C., 1996, Nature, 380, 606
- Machida M. N., Inutsuka S., Matsumoto T., 2010, ArXiv e-prints
- Masunaga H., Inutsuka S.-i., 2000, ApJ, 531, 350
- McCrea W. H., 1960, Royal Society of London Proceedings Series A, 256, 245
- McCrea W. H., Williams I. P., 1965, Royal Society of London Proceedings Series A, 287, 143
- Meru F., Bate M. R., 2010, ArXiv e-prints
- Nayakshin S., 2010a, ArXiv e-prints, 1007.4159
- Nayakshin S., 2010b, ArXiv e-prints, 1007.4165
- Nayakshin S., 2010c, ArXiv e-prints, 1007.4162
- Nayakshin S., Cha S.-H., Hobbs A., 2009, MNRAS, 397, 1314
- Pollack J. B., Hubickyj O., Bodenheimer P., Lissauer J. J., Podolak M., Greenzweig Y., 1996, Icarus, 124, 62
- Rafikov R. R., 2005, ApJL, 621, L69
- Rice W. K. M., Lodato G., Armitage P. J., 2005, MNRAS, 364, L56
- Safronov V. S., 1969, Evoliutsiia doplanetnogo oblaka.
- Springel V., 2005, MNRAS, 364, 1105
- Stamatellos D., Whitworth A. P., 2008, A&A, 480, 879
- Tanaka H., Takeuchi T., Ward W. R., 2002, ApJ, 565, 1257
- Vorobyov E. I., Basu S., 2005, ApJL, 633, L137
- Vorobyov E. I., Basu S., 2006, ApJ, 650, 956
- Vorobyov E. I., Basu S., 2010, ArXiv e-prints
- Weidenschilling S. J., 1977, MNRAS, 180, 57
- Weidenschilling S. J., 1980, Icarus, 44, 172
- Wetherill G. W., 1990, Annual Review of Earth and Planetary Sciences, 18, 205
- Williams I., Crampin D. J., 1971, MNRAS, 152, 261
- Youdin A. N., Goodman J., 2005, ApJ, 620, 459

## APPENDIX A: CONTRACTION OF THE GRAIN CORE

The size of the grain core in our simulations can be smaller than the SPH smoothing length in the centre of the gas clump (see §4.2). There is then a concern about proper numerical treatment of the gravitationally contracting dust grain core: perhaps the formation of the “Super-Earth core” is somehow artificial and is due to our final SPH resolution.

We believe that an improved SPH resolution would not hinder grain sedimentation into a self-bound core. To back up this statement, and on the referee’s suggestion, we have performed several made-to-purpose simulations. To this end, we have selected the “S” clump that contained the Super-Earth core to initialise these test runs. The selection was done at time of  $t = 4880$  yrs (same as Figure 7). We then re-sampled the SPH particle distribution to change the SPH particle number, which was varied from one quarter to twice the original SPH particle number. We also varied  $h_{min}$ , the gravitational softening for the dust component, increasing and decreasing it by a factor of 2. The “Super-Earth” clump was then re-simulated for 500 years.

As we expected (see below), the number of SPH particles did not have a critical influence on the results, whereas changes in the  $h_{min}$  were critical. As we stated in §4.2, improving our numerical resolution in treating the self-gravity of the dust (decreasing  $h_{min}$ ) should result in further decrease in the size of the grain core, and in the limit of  $h_{min} \rightarrow 0$  it should contract to a point. Increasing  $h_{min}$ , degrading numerical resolution of the gravity force, should result in a more extended grain core.

Fig. A1 shows the innermost 0.003 AU for 4 of these



tests at 500 yrs. This region contains most of the dust grain particles of the Super-Earth core. The panel C2 shows the results for the test with the same number of SPH particles and  $h_{min} = 0.05$  AU as presented elsewhere in the paper. The panel C3 and D3 has  $h_{min} = 0.02$  AU. The panel D2 and D3 have twice the SPH particle number of the original simulation (C2). D2 has  $h_{min} = 0.05$  AU, as C2.

From the Figure, we see that decreasing  $h_{min}$  leads to a correspondg decrease in the size of the dust core, as should be. At the same time, improving the SPH resolution hardly changes the size of the dust concentration, which has a simple explanation. Within the centre of the clump, our dust-gas neighbour treatment (Nayakshin et al. 2009) leads to a constant density field on scales smaller than the SPH smoothing length. Thus the grain-gas drag does not “disappear” or gets reduced in the centre of the clump on arbitrarily small scales.

However, due to a finite numerical resolution, we could still miss some effects on small scales. For example, if the mass of the solids in this small scale region is very high, say 20 Earth masses, the gas itself could be influenced by the gravity of the dust particles (Nayakshin 2010a,c). The gas could then build-up to higher densities around the dust core. In the final disruption of the embryo some of this inner gas envelope could then survive. We regret to say that at this point we cannot resolve such small scales. However it would seem that these effects would make the solid core even more gravitationally bound, due to the increased mass in the region.

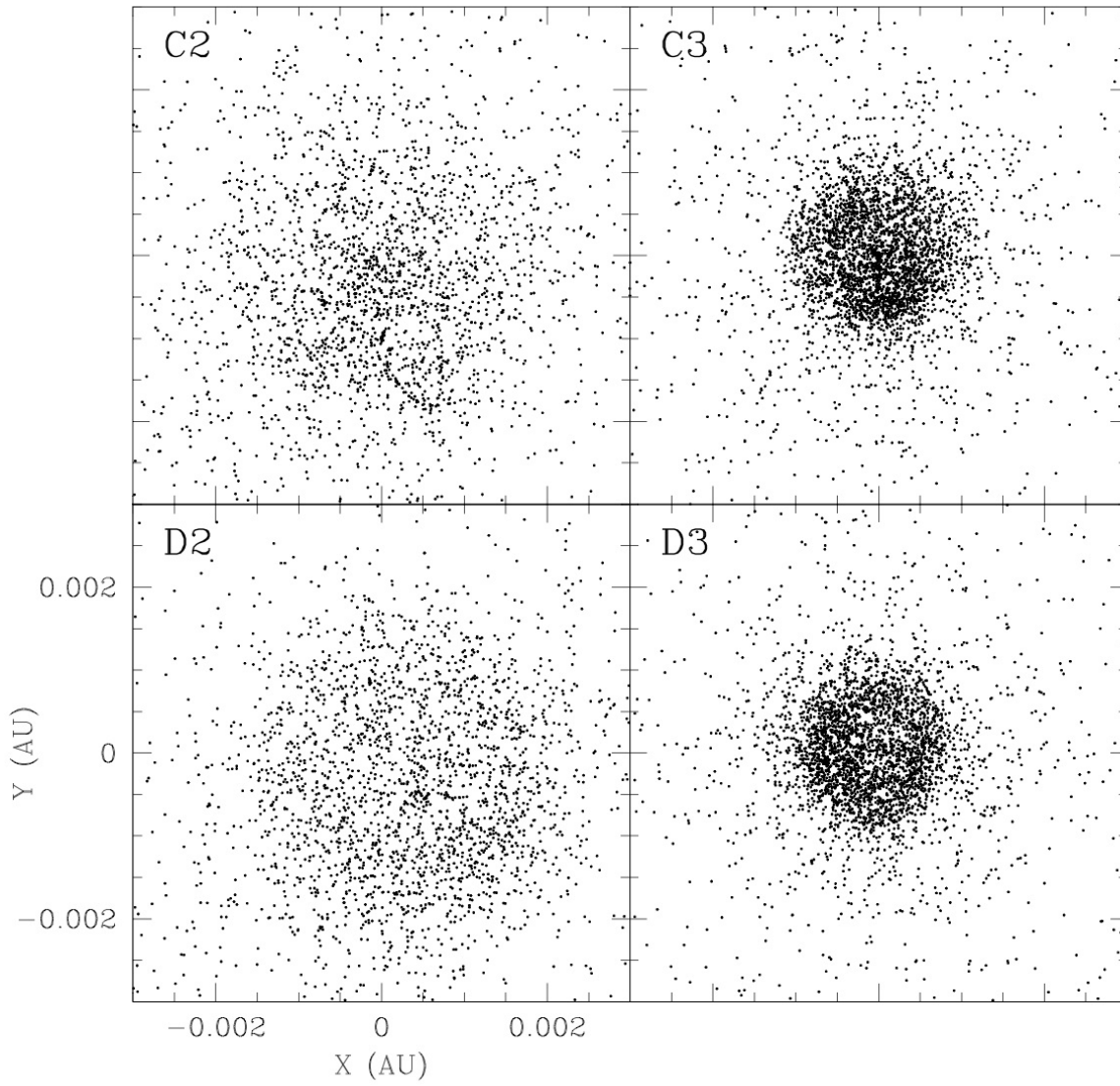


**Figure A1.** The isolated clump simulations performed to check the numerical validity of grain sedimentation.